





## Persistent double strand break accumulation does not precede cell death in an Olaparib-sensitive BRCA-deficient colorectal cancer cell model

Natalia Soledad Paviolo<sup>1\*</sup>, María Belén de la Vega<sup>1\*</sup>, María Florencia Pansa<sup>2,3</sup>, Iris Alejandra García<sup>2,3</sup>, Nicolás Luis Calzetta<sup>1</sup>, Gastón Soria<sup>2,3</sup>  and Vanesa Gottifredi<sup>1</sup> 

<sup>1</sup>Fundación Instituto Leloir-Instituto de Investigaciones Bioquímicas de Buenos Aires. Buenos Aires, Argentina.

<sup>2</sup>Centro de Investigaciones en Bioquímica Clínica e Inmunología, CIBICI-CONICET. Córdoba, Argentina.

<sup>3</sup>Departamento de Bioquímica Clínica. Facultad de Ciencias Químicas, Universidad Nacional de Córdoba. Córdoba, Argentina.

### Abstract

The poly (adenosine diphosphate (ADP)-ribosyl) polymerase inhibitors (PARPi) selectively kill cancer cells with BRCA1 or BRCA2 (BRCA)-mutations. It has been proposed that cell death induction after PARPi depends on unrepaired double strand breaks (DSBs) that accumulate due to the homologous recombination deficiency of BRCA-mutated cells. Such accumulation of DSBs is inferred mainly from the high levels of DNA damage markers like phosphorylated histone H2AX. Herein, we developed a model of isogenic cell lines to show that depletion of BRCA causes PARPi-triggered cell death, replication stress (phosphorylated-H2AX and 53BP1 foci), and genomic instability. However, persistent DSBs accumulation was not detected under the same experimental conditions. Hence, at least in this cellular model, the trigger for cell death in PARPi-treated BRCA-depleted samples is not the accumulation of unrepaired DSBs. Instead, cell death better correlates with a rapid and aberrant resolution of DSBs by error-prone pathways that leads to severe chromosomal aberrations. Therefore, our results suggest that in PARPi-treated BRCA-deficient cells, chromosome aberrations may dually trigger both genomic instability and cell death.

**Keywords:** GammaH2AX, alternative end joining, non-homologous end joining, homologous recombination, PARP.

Received: February 28, 2019; Accepted: May 5, 2019.

### Introduction

Homologous recombination (HR)-deficiency leads to genomic instability due to the shift from “error-free” to “error-prone” DNA repair pathways (Prakash *et al.*, 2015; Talens *et al.*, 2017). HR-deficiency is, therefore, a driver of tumorigenesis as demonstrated in cancer cells deficient in BRCA1- and BRCA2 (BRCA) expression or functions (Fackenthal and Olopade, 2007; Ramus and Gayther, 2009). The HR-deficiency was also detected in BRCA1/2-proficient cells. Such a condition is currently defined as BRCAness of a tumor (Lord and Ashworth, 2016). The BRCAness phenotype is frequently found in breast, ovarian, pancreatic, prostatic, and other types of cancers (Alexandrov *et al.*, 2015; Holter *et al.*, 2015; Robinson *et al.*,

2015; Waddell *et al.*, 2015; Davies *et al.*, 2017). Given the selective acquisition of BRCAness in tumors but not in healthy cells, therapeutic targets that specifically kill HR-deficient tumors but not proficient cells from patients were explored. Such a synthetic lethality (SL) approach has already transcended from academic laboratories to pharmaceutical companies. Poly [adenosine diphosphate (ADP)-ribosyl] polymerase inhibitors (PARPi) were developed to selectively increase cell killing of HR-deficient cancer cells sparing HR-proficient cells (Lord and Ashworth, 2017). Notably, four PARP inhibitors are already available for clinical use (Olaparib from AstraZeneca approved in 2015, Rucaparib from Clovis approved in 2016, Niraparib from TESARO/GSK approved in 2017, and Talazoparib from Pfizer approved in 2018). Moreover, the optimization of PARPi is still a subject of current research, and it is thus possible that other PARPi will be approved for clinical use in the near future (Sun *et al.*, 2018).

Despite their current success in the clinical setting, the mechanism of action of PARPi has only been partially elucidated. While it is accepted that double-strand breaks

Send correspondence to Gastón Soria, Universidad Nacional de Córdoba, Av. Haya de la Torre s/n, Córdoba, Argentina. Phone/Fax: 54-351-5353850, ext. 55316; E-mail: [gsoria@fcq.unc.edu.ar](mailto:gsoria@fcq.unc.edu.ar); and Vanesa Gottifredi, IIBBA, Fundación Instituto Leloir, CONICET, Av. Patricias Argentinas 435, C1405 BWE, Buenos Aires, Argentina. E-mail: [VGottifredi@leloir.org.ar](mailto:VGottifredi@leloir.org.ar).

\*These authors contributed equally to this study.

(DSBs) are frequently formed in BRCA-deficient cells, the trigger of such DNA lesions is a subject of debate. Originally, the SL induced by PARPi was attributed to the inhibition of base excision repair (BER) (Bryant *et al.*, 2005; Farmer *et al.*, 2005). PARPi-mediated inhibition of BER was proposed to trigger DSBs when unresolved single-strand breaks on DNA are encountered by replication forks in S-phase. Such replication-associated DSBs are expected to be toxic in the absence of HR. However, contrasting evidence showed that BER deficiency, and even PARP knock-out, do not recapitulate the phenotypes caused by PARPi (Helleday, 2011). Instead, the trapping of the PARP enzymes in the regions of DNA damage seems to be the synthetic lethal event triggered by PARPi. When encountered by the replisome, such persistent PARP/DNA complex triggers stalling, collapse and breakage of replication forks into DSBs (Pommier *et al.*, 2016). Hence, both previous and current models suggest that the cause of SL triggered by PARPi depends on the accumulation of DSBs.

A different line of evidence demonstrates that replication-associated DSBs are formed after PARPi treatment. Chromosome aberrations generated at DSBs accumulate in BRCA-depleted samples treated with PARPi (Farmer *et al.*, 2005). Moreover, the genomic signature of BRCAness also requires DSB formation (Davies *et al.*, 2017). However, the evidence of DSB persistency so far accumulated in the literature is almost exclusively related to the analysis of cells with  $\gamma$ H2AX, 53BP1, and Rad51 nuclear foci (Bryant *et al.*, 2005; Farmer *et al.*, 2005; Rottenberg *et al.*, 2008; Jaspers *et al.*, 2013; Johnson *et al.*, 2013; Michl *et al.*, 2016). Here we use an isogenic system to downregulate either BRCA1 or BRCA2 in colorectal cells, both of which showed strong sensitivity to Olaparib. As reported in other cellular models, the fraction of cells with numerous  $\gamma$ H2AX and 53BP1 foci was upregulated in BRCA-depleted samples treated with Olaparib, and such replication stress was followed by chromosome instability. However, the neutral comet assay did not reveal a significant upregulation of DSBs in Olaparib-treated BRCA samples. Together, these results suggest that DSB formation but not its persistency precede both cell death and genomic instability in Olaparib treated BRCA-deficient cells.

## Material and Methods

### Cell lines and cell culture

HCT116<sup>p21<sup>-/-</sup></sup> cells were generated (Bunz *et al.*, 1998) and kindly provided by B. Vogelstein. Cell culture was performed in DMEM medium (Thermo Fisher Scientific) supplemented with 10% FBS (GIBCO-NZ) and 1% penicillin-streptomycin. Control for mycoplasma contamination was performed periodically with a PCR-based method with internal loading control. To generate cell lines expressing fluorescent proteins, all the fluorescent proteins were expressed from the same backbone from Clontech as de-

scribed in Carbajosa *et al.* (2019). Briefly, transfection of vectors encoding fluorescent proteins (piRFP-C1, pECFP-C1, pmCherry-C1) was performed using JetPrime (Polyplus-transfection) according to manufacturer's instructions. After multiple rounds of cell sorting (3-5) performed with FACS Aria II (BD bioscience), stable cell line pools expressing the different fluorescent proteins were established. The resulting cell lines pools were transduced with control, shBRCA1, and shBRCA2 using titers that promoted the higher downregulation BRCA1 and BRCA2 by qPCR and WB, yet keeping similar proliferation rates to the shSCR-transduced cell lines. Our goal here was to avoid clonal selection, which is often an issue that could result in misleading conclusions when generating stable cell lines. shSCR, shBRCA1, and shBRCA2 cell lines were used for experimentation for no more than six passages after the establishment of the cellular pools.

### DNA constructs and shRNA

shBRCA1 (TRCN0000010305, Sigma-Aldrich) and shBRCA2 (Carlos *et al.*, 2013), were cloned into pLKO.1-TRC vector through *EcoRI* and *AgeI* restriction sites; and shSCR-pLKO.1 was previously described (46). shSCR-plenti (TR30021), was acquired from Origene.

### Antibodies

Primary antibodies used were:  $\alpha$ -BRCA1 (Oncogene Research), KU70 (Abcam),  $\alpha$   $\gamma$ H2AX Ser 139, Upstate (Millipore, clone JBW301),  $\alpha$  53BP1 (Santa Cruz). Secondary antibodies used were Anti-mouse IgG (Sigma-Aldrich A 4416) for western blot analysis and  $\alpha$ -mouse/rabbit-conjugated Cy2/Cy3 antibodies (Jackson Immuno Research) for immunofluorescence assays. Nuclei were stained with DAPI (Sigma).

### Cell counting methods

Cells were seeded on 96-well dishes at a density of 1500 cells/well. Cells were fixed with 2% paraformaldehyde/sucrose. InCell 2200® was used to obtain images of DAPI-stained nuclei and an InCell Analyzer WorkStation® was used to count nuclei. Alternatively, the number of viable HCT116 p21<sup>-/-</sup> shBRCA1/2 and shSCR cells was determined with a CellTiter-Glo® Luminescent Cell Viability Assay G-7570 (Promega), according to the manufacturer's instructions. When assessing growth rates, cells stably expressing iRFP were seeded in 96-well plate at  $2 \times 10^3$  cell/well and plates were scanned daily in the Odyssey Clx System (LI-COR Biosciences) as previously reported (Hock *et al.*, 2014). For flow cytometry experiments, isogenic cell populations were counted using a Countess FL device (Thermo Fisher) previous to plating the co-cultures.

## Co-cultivation method

Transfection protocols were performed using JetPrime (Polyplus-transfection) according to the manufacturer's instructions. Multiple rounds of cell sorting (3-5) were performed (FACS Aria II, BD Bioscience) to select pools that express CFP, iRFP, and mCherry fluorescent proteins. Each "colored" cell line was sub-sequentially used to generate shSCR, shBRCA1, and shBRCA2 expressing pools (Carbajosa *et al.*, 2019). The transduced cells that showed the higher downregulation of BRCA1 and BRCA2 by qPCR and WB, yet keeping similar proliferation rates to the shSCR-transduced cell lines, were selected for survival assays. Equal amounts of cells were plated in a single 96 well ensuring ~33% distribution for each cell line. As a consequence of the equal proliferation rate, such distributions were conserved at the endpoint, which took place 6 days later. SL treatment alters the composition in a way that the proportion of shSCR increases and the shBRCA1 and shBRCA2 decrease.

## Cell cycle analysis

Cells were fixed with ice-cold ethanol and re-suspended in PBS containing RNase I (100 mg/mL, Sigma) and propidium iodide (50 mg/mL, Sigma). Samples were subjected to fluorescence-activated cell sorting (FACS, Calibur, Becton Dickinson), and data were analyzed using the Summit 4.3 software (DAKO Cytomation) as previously described (Federico *et al.*, 2016).

## Protein analysis

For direct western blot (WB) analysis, samples were lysed in commercial Laemmli buffer (Bio-Rad) containing the reducing agent 2-mercaptoethanol. ECL detection (Amersham, GE Healthcare) was performed according to the manufacturers' instructions. Western blot images were taken with Image QuantLAS4000 (GE Healthcare), which allows capture and quantification of images within a linear range.

## Quantitative RT-PCR

Cells were lysed and total RNA was extracted using TRIzol® Reagent (Invitrogen). Reverse transcription was performed and BRCA2 mRNA levels were measured with Fw-5'-AGGGCCACTTTCAAGAGACA3' and Rv-5'TAGTTGGGGTGGACCACTTG3' primers using the iQ SYBR Green Supermix (Invitrogen). Relative expression levels were normalized to GAPDH.

## Immunostaining and microscopy

Cells were fixed in 2% (w/v) paraformaldehyde (PFA)/2% sucrose and permeabilized with 0.1% (v/v) Triton X-100 in phosphate buffered saline (PBS). Blocking during 2 h at RT in PBS 2% (v/v) donkey serum (Sigma) was performed. Coverslips were incubated for 1 h in primary antibodies and then 1 h in secondary antibodies. Im-

ages were obtained with a Zeiss Axioplan confocal microscope or a Zeiss Axio Imager.A2. A total of 250-300 nuclei were analyzed per sample following the procedure described in (Mansilla *et al.*, 2016).

## Chromosomal aberration analysis

Metaphase chromosome spreads were generated introducing minor modifications to protocols previously used by us (Federico *et al.*, 2016). Before harvesting, cells were treated with Colcemid (0.08 µg/mL, KaryoMAX, Invitrogen) for 3 h. Cell pellets were incubated in hypotonic buffer (KCl 0.0075 M) at 37 °C for 4 min, followed by fixation in Carnoy's fixative (3:1 methanol: glacial acetic acid). Cells were dropped onto slides and air-dried before staining with 6% (w/v) Giemsa in Sorensen's buffer (2:1 67 mM KH<sub>2</sub>PO<sub>4</sub> : 67 mM Na<sub>2</sub>HPO<sub>4</sub>, pH 6.8) for 2 min. 70 metaphase spreads were evaluated to detect gaps, breaks, and exchanges using an Applied Imaging Cytovision (2.10.17 version, Leica).

## Micronucleus (MN) assay

Cells seeded at low density were treated. Micronuclei analysis was performed using protocols previously described previously by us (Federico *et al.*, 2016). Samples were incubated with cytochalasin B (4.5 µg/mL, Sigma) for 36 h. Cells were washed for 1 min with hypotonic buffer (KCl 7.5 mM), twice with PBS and fixed with PFA/sucrose 2% for 20 min. DAPI staining served to visualize whole cells and nuclei respectively. 300 binucleated cells were analyzed and the frequency was calculated as MN/binucleated cells.

## Neutral comet assay

We used protocols previously described by Murfun *et al.* (2013) with some modifications. Briefly, cells were embedded in 0.5% low-melting agarose on a slide and treated with a lysing solution (EDTA 30mM, SDS 0.5%) for 10 min at 4 °C. Slides were washed twice with deionized water (ddH<sub>2</sub>O), immersed in TBE 1X and subjected to electrophoresis at 17 V (6-7 mA) during 5 min at 4 °C. Samples were washed with ddH<sub>2</sub>O and stored in methanol overnight DNA was stained with propidium iodide and samples were examined with a Zeiss fluorescence microscope. To determine the tail moment (tail length x fraction of total DNA in the tail), 100-150 nuclei were evaluated per each condition using the OpenComet program.

## Statistical analysis

Statistical analyses were performed using GraphPad Prism 5.0 (GraphPad Software), applying the Student's *t*-test and ANOVA test as appropriate. Graphs were generated using the same software.

## Results

### Downregulation of BRCA1 or BRCA2 levels sensitizes HCT116 colorectal cancer cells to Olaparib treatment

Generating BRCA-deficient cell lines by stable knockdown is a difficult process, as most cells do not survive in the long term. The main limitation to reach stable BRCA depletion is the abrupt proliferation arrest that follows a severe knockdown or depletion of BRCA (Feng and Jasin, 2017). In order to achieve an efficient knockdown of BRCA proteins, we set up an shRNA-based downregulation of BRCA1 or BRCA2. Many cell lines did not recover after an acute crisis, and other cell lines regained BRCA expression after a few passages (Carvajosa *et al.*, 2019). We then explored colorectal cancer cells that are not characterized by a high frequency of BRCA loss. We chose a modified HCT116 cell line lacking the cyclin kinase inhibitor p21 that, therefore, has an attenuated G1/G2 checkpoint (Bunz *et al.*, 1998), which could favor the establishment of stable BRCA-deficient cells. It should be also mentioned that p21 deficiency negatively regulates BRCA2-mediated repair of replication-coupled DSBs (Mauro *et al.*, 2012), which could be relevant for controlling BRCA1 deficient but not BRCA2 deficient cells. As described in the methods sections we set up a protocol that efficiently downregulated BRCA1 and BRCA2 (Figure 1A). In contrast to other cells lines tested, HCT116<sup>p21<sup>-/-</sup></sup> showed similar proliferation rates on BRCA-proficient and BRCA-deficient cells (Figure 1B). Flow cytometry analysis showed a strong BRCA1/2-related cell cycle arrest and subG1 accumulation in BRCA-depleted samples (Figure 1C). Synthetic lethality (SL) induction after Olaparib treatment was observed at 6 days post-Olaparib treatment in single cultivation methods and co-cultivation experiments (Figure 1D-G). The SL correlated with the efficiency of BRCA1 downregulation, reaching a critical level at passage 10 (Figure 1H). Hence, colorectal cancer cells, which do not frequently lose BRCA, can be sensitized to Olaparib by BRCA knockdown.

### Olaparib-triggered cell death in BRCA-deficient samples is preceded by the accumulation of markers of double-strand break formation and repair

Many reports indicate that the treatment of BRCA-deficient cells with PARPi triggers an acute increase of replication stress that leads to the accumulation of DSBs. Such DSBs were frequently revealed as  $\gamma$ H2AX foci formation in the nucleus of PARPi-treated cells (Bryant *et al.*, 2005; Farmer *et al.*, 2005; Rottenberg *et al.*, 2008; Jaspers *et al.*, 2013; Johnson *et al.*, 2013; Michl *et al.*, 2016). In our experimental settings, the percentage of cells with high levels of  $\gamma$ H2AX foci significantly increased at 2 days after Olaparib treatment (Figure 2A,B), which is in agreement with previous reports. The percentage of cells with  $\gamma$ H2AX de-

creases after that time, reaching levels that are similar to those of untreated conditions at 6 days (not shown). The localization of 53BP1 to nuclear foci also increased in the same experimental conditions and at 48 hours after Olaparib treatment (Figure 2C,D). Such observations suggested that in HCT116<sup>p21<sup>-/-</sup></sup> cells depleted from BRCA proteins, acute replication stress precedes the cell death triggered by PARPi. Moreover, the rapid recruitment of 53BP1 to such DSBs indicates that DSBs could be rapidly repaired by a 53BP1-driven repair.

### Olaparib-triggered cell death in BRCA-deficient HCT116<sup>p21<sup>-/-</sup></sup> is preceded by accumulation of chromosome instability

In the context of BRCA-depletion, 53BP1 favors the repair of DSBs by non-homologous end joining (NHEJ) (Daley and Sung, 2014). Since PARPi-induced DSBs are actually one-ended DSBs formed at the tip of collapsed replication forks, the NHEJ-mediated processing of such DSBs indefectible causes formation of radial chromosomes and increase other types of chromosome instability (Federico *et al.*, 2018). In agreement with results obtained in mammary and ovarian models, the depletion of BRCA proteins in HCT116<sup>p21<sup>-/-</sup></sup> colorectal cancer cells cause massive genomic instability after Olaparib treatment. Such genomic instability was manifested as the extensive accumulation of gaps, breaks, radial chromosomes (Figure 3A,B) and micronuclei (Figure 3C,D), which are all markers of aberrant repair of DSBs (Federico *et al.*, 2018). Together these experiments show that a steep increase in genomic instability temporally precedes cell death in PARPi-treated HCT116<sup>p21<sup>-/-</sup></sup> cells.

### Olaparib-triggered cell death in BRCA-deficient samples is not preceded by persistent double-strand breaks

While the accumulation of cells with  $\gamma$ H2AX foci is accepted as a marker of DSB accumulation in many PARPi-related studies, experts in the field have addressed the limitations of such markers (Zellweger *et al.*, 2015). Intriguingly, the maximum percentage of cells with  $\gamma$ H2AX foci was observed at 2 days after Olaparib treatment (Figure 2B) although cell death was negligible even at 3 days after Olaparib treatment (Figure 1C). Hence, we wondered whether DSBs formed at the time of maximal  $\gamma$ H2AX detection would accumulate for a long time to eventually trigger cell death days later. We reasoned that direct detection of DSBs should be set up, and so we optimized the neutral comet assay to be used in our experimental conditions. Bleomycin was used as a positive control to observe the accumulation of DSBs in HCT116<sup>p21<sup>-/-</sup></sup> cells (Figure 4A). Surprisingly, DSBs were not detected by neutral comet assay after Olaparib treatment in both BRCA-deficient cell lines (Figure 4B,C). Ruling out the possibility of a delayed accumulation of DSBs, the neutral comet assay did not reveal

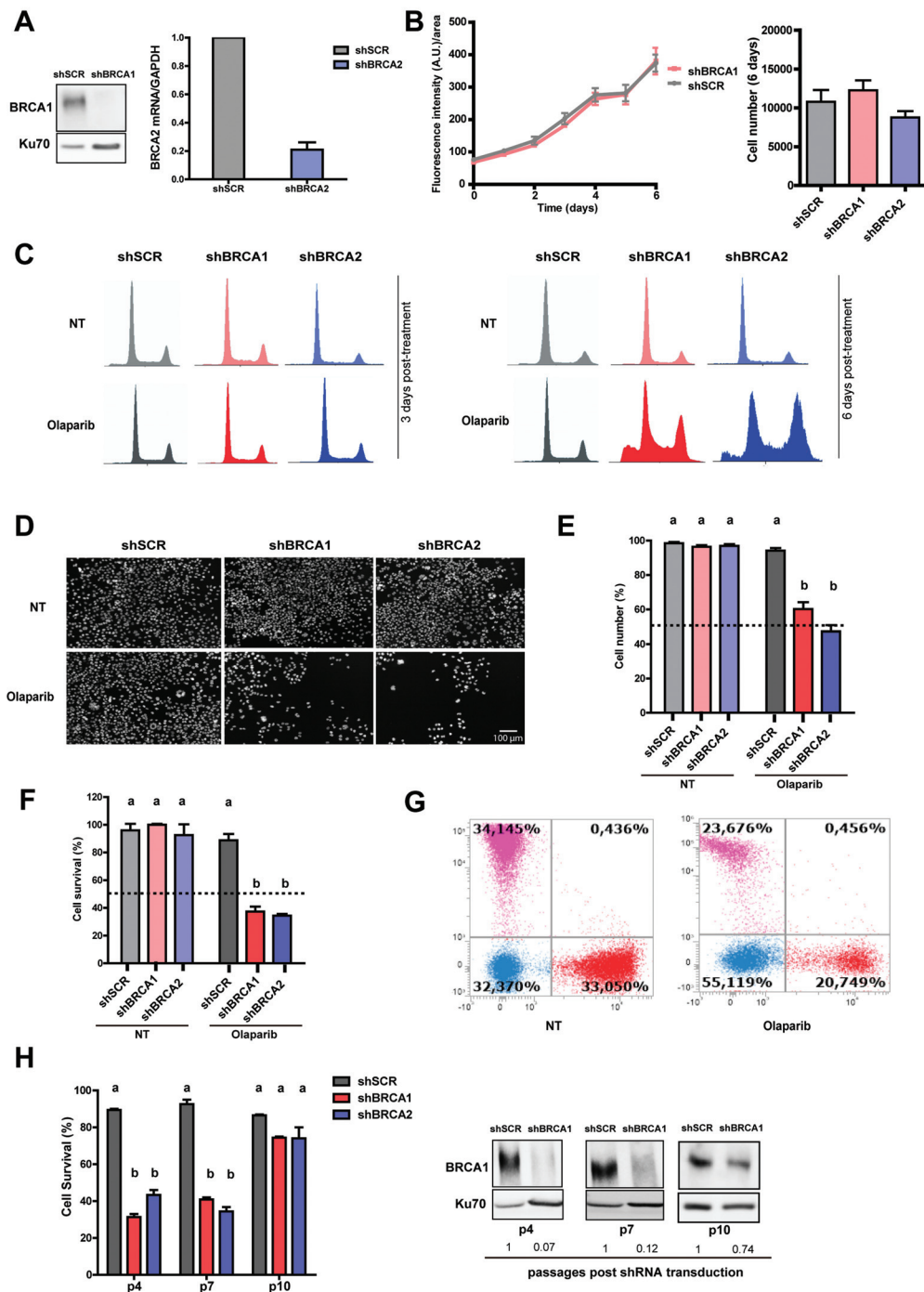


**Figure 1** - BRCA1 and BRCA2 downregulation sensitize colorectal cancer HCT116<sup>p21-/-</sup> cells to Olaparib treatment. A) HCT116<sup>p21-/-</sup> were transduced with control (shSCR\_scramble) and shRNA vectors specific for BRCA1 and BRCA2 (shBRCA1 and shBRCA2). Western blot and RT-qPCR showing the levels of BRCA1 and BRCA2 protein and mRNA, respectively, at passage 4 after transduction. B) Growth curves of untreated samples. Data are shown as mean ± SD from 5 independent experiments. C) Flow cytometry of propidium iodide-stained samples. D) Representative panels depicting the SL induced in the HCT116<sup>p21-/-</sup> cells after BRCA downregulation. Samples were stained with DAPI and photographs were obtained after automatic capture. E-F) HCT116<sup>p21-/-</sup> cells transduced with shSCR and shRNA vectors specific for BRCA1 and BRCA2 (shBRCA1 and shBRCA2) were plated at a density of 1500 cells/well in 96 well plates. Six days later, samples were counted with direct (automated cell counter-E) and indirect (F-cell titer Glo) methods. The plot shows the quantification (mean ± SD) of the surviving fraction of 3 independent experiments. G) HCT116<sup>p21-/-</sup> cells were transduced with fluorescent proteins to generate colored pools as described in the material and methods section. After shRNA transduction, samples were co-cultured and treated with Olaparib when indicated. The plot shows the quantification of the surviving fraction of 3 independent experiments. H) Synthetic lethality (SL) is lost with increasing cell passages (mean ± SD, n = 2). Western blot showing BRCA1 levels at different times post shRNA transduction. Numbers below each lane are the quantification of normalized BRCA1 levels. Cell number was determined at the indicated passages and the SL was calculated. Statistical analysis was performed using two-way ANOVA with Bonferroni post-hoc test and differences were considered significant with  $p \leq 0.001$ . The letters above the different values indicate groups that are significantly different.

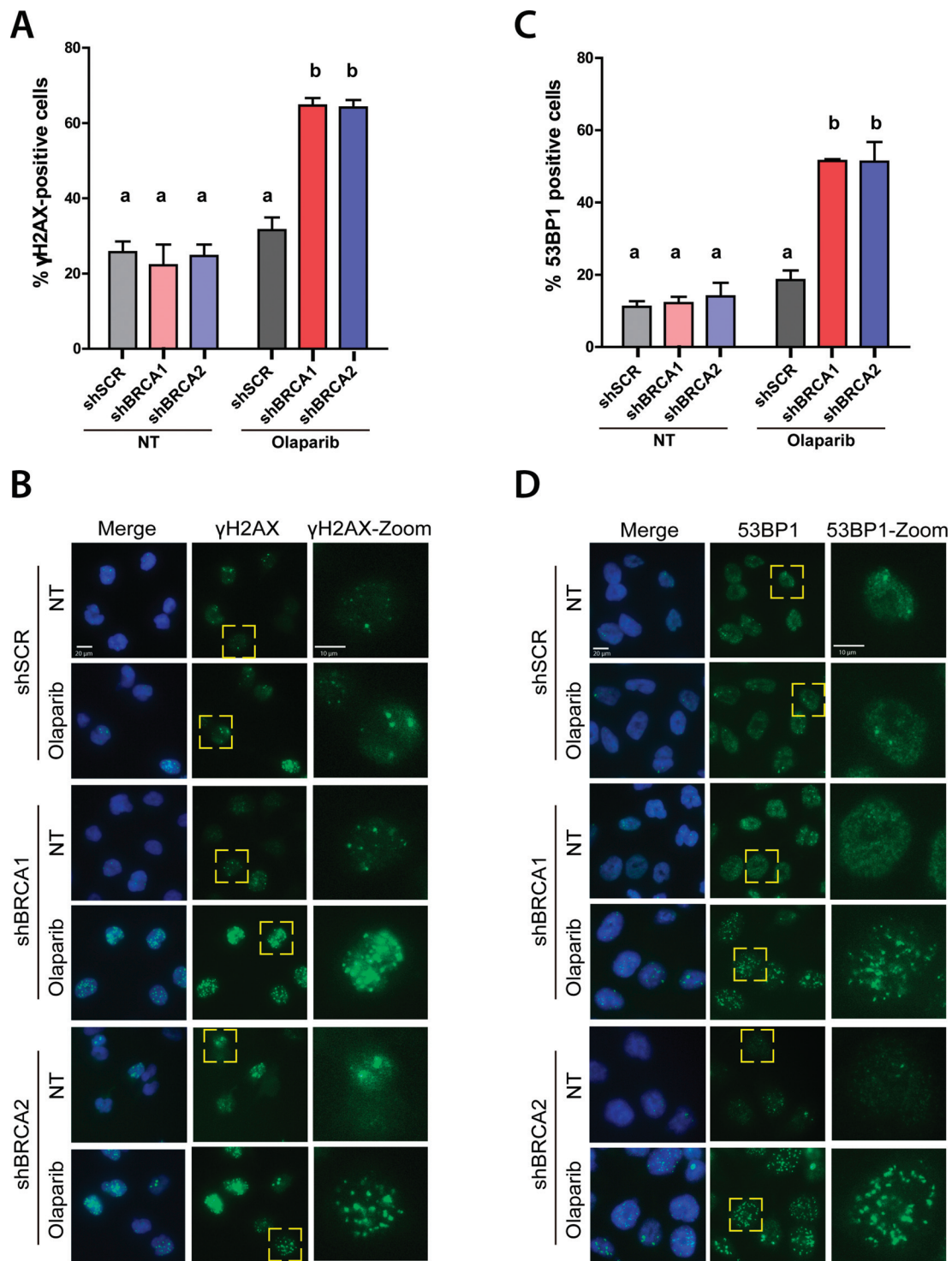


**Figure 2** - The number of cells with  $\gamma$ H2AX and 53BP1 foci in BRCA-depleted HCT116<sup>p21-/-</sup> cells increases after Olaparib treatment. A) HCT116<sup>p21-/-</sup> cells transduced with shSCR, shBRCA1, and shBRCA2 cells were treated with Olaparib. After 48 h, immunostaining with  $\gamma$ -H2AX antibodies was performed. The percentage of cells with foci was quantified using fluorescence microscopy (magnification: 100X). Nuclei with more than 35  $\gamma$ H2AX focal structures were considered positive. At least 300 cells per condition were analyzed in 5 independent experiments. Statistical analysis was performed using Two-way ANOVA with Bonferroni post-hoc test ( $***p \leq 0.001$ ). Data are shown as mean  $\pm$  SD. B) Representative images of data showed in A. Zoom images of the nuclei indicated with the yellow dotted square are showed on the left. C) HCT116<sup>p21-/-</sup> shSCR and shBRCA1 cells were treated with Olaparib. After 48 h, immunostaining with a 53BP1 antibody was performed. The percentage of cells with foci was quantified using fluorescence microscopy (magnification: 100X). Only nuclei with more than five 53BP1 foci were quantified as positive. At least 300 cells per condition were analyzed and data are shown as mean  $\pm$  SD from 5 independent experiments. D) Representative images of data showed in C. Zoom images of the nuclei indicated with the yellow dotted square are showed on the left. Statistical analysis was performed using Two-way ANOVA with Bonferroni post-hoc test and differences with  $p \leq 0.001$  were considered significant. In all graphs, the letters above the different values indicate groups that are significantly different.

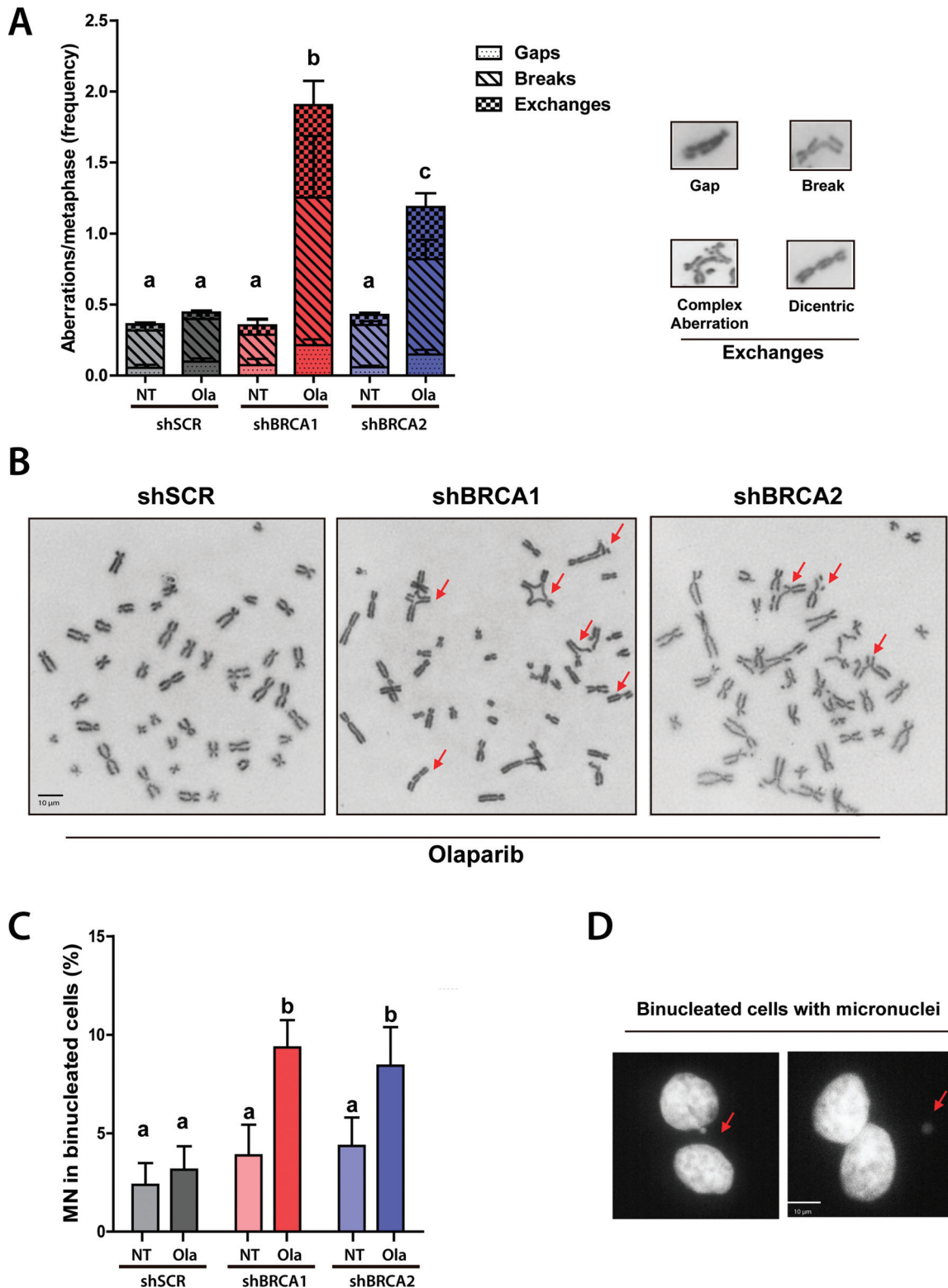


**Figure 3** - Chromosome instability precedes Olaparib-triggered cell death in BRCA-deficient HCT116<sup>p21-/-</sup>. **A**) HCT116<sup>p21-/-</sup> cells transduced with shSCR, shBRCA1 and shBRCA2 were submitted to cytogenetic analysis 48 h after the treatment with Olaparib. The frequency of gaps, breaks, and exchanges was calculated after analyzing a minimum of 70 metaphases per condition in 5 independent experiments. **B**) Representative images of chromosomal aberrations quantified in **A**. **C**) HCT116<sup>p21-/-</sup> transduced with shSCR, shBRCA1 and shBRCA2 were treated for 24 h with Olaparib and were arrested at a binucleated stage using cytochalasin B. The frequency of micronuclei was estimated (shown as mean  $\pm$  SD, using DAPI staining and fluorescence microscopy (magnification: 100X), analyzing a minimum of 300 binucleated cells per condition in 4 independent experiments. **D**) Representative images of chromosomal aberrations quantified in **C**. Statistical analysis was performed using two-way ANOVA with Bonferroni post-hoc test and differences were considered significant with  $p \leq 0.001$ . The letters above the different values indicate groups that are significantly different.

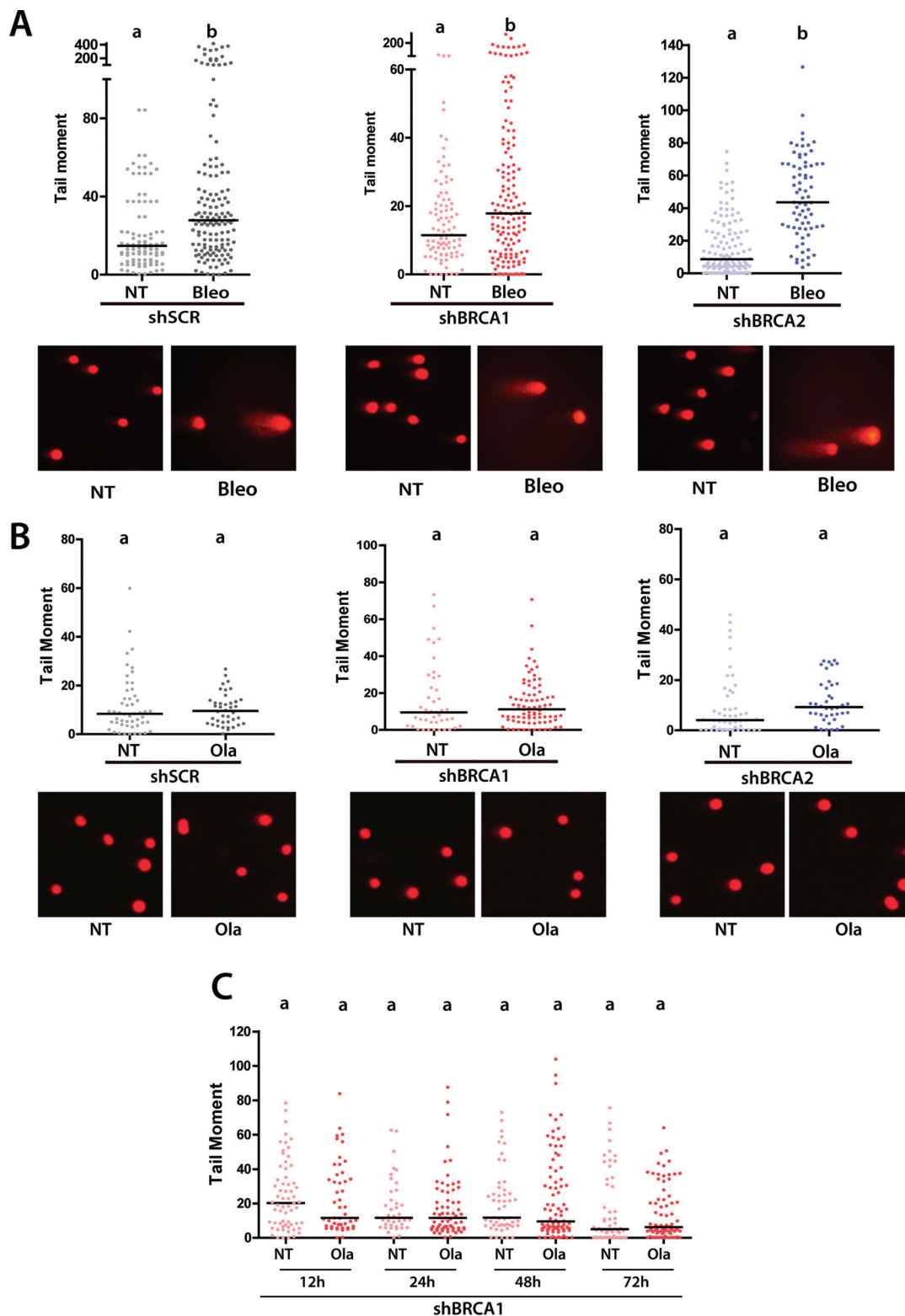


**Figure 4** - Persistent double-strand break accumulation does not precede Olaparib-triggered cell death in BRCA-deficient HCT116<sup>p21-/-</sup> cells. A) HCT116<sup>p21-/-</sup> cells transduced with shSCR, shBRCA1 and shBRCA2 were submitted to neutral comet assay in untreated and Bleomycin-treated conditions (mean +SD, n= 2). B) HCT116<sup>p21-/-</sup> cells transduced with shSCR, shBRCA1 and shBRCA2 were submitted to neutral comet assay two days after Olaparib treatment, which coincides with the maximum levels of  $\gamma$ H2AX accumulation. Results are representative of 2 independent experiments. C) HCT116<sup>p21-/-</sup> cells transduced with shSCR and shBRCA1 were submitted to neutral comet assay at the indicated days after Olaparib treatment. Results are representative of 2 independent experiments. Statistical analysis was performed using One Way ANOVA with Dunns comparison test and differences were considered significant with  $p \leq 0.05$ . The bars on top of the distribution clouds indicate the median. The letters above the different values indicate groups that are significantly different.



DSBs at any time points after Olaparib treatment (Figure 4C). Together, these results demonstrate that persistent accumulation of DSBs is not frequent in Olaparib-treated BRCA-deficient HCT116<sup>p21<sup>-/-</sup></sup> cells. Hence, cell death is unlikely triggered by unrepaired DSBs in these settings. Instead, DSBs may indirectly trigger cell death in a manner that depends on the accumulation of unstable chromosomes generated by dysregulated error-prone pathways (Figure 5). Together, these results show that genomic instability and cell death are intimately associated with BRCA-deficient HCT116<sup>p21<sup>-/-</sup></sup> cells treated with PARPi. The implications of these findings for the acquisition of resistance in PARPi treated BRCA cancers will be discussed below.

## Discussion

The accumulation of unrepaired DSBs is considered to be the trigger of cell death in BRCA-deficient cells treated with PARPi (Bryant *et al.*, 2005; Farmer *et al.*, 2005). However, at least in the isogenic cellular model presented in this study, BRCA-depletion triggered cell death and chromosome instability but not detectable DSB accumulation. Such a finding suggests that the cause of cell death in this scenario is not mainly associated with the persistence of unrepaired DSBs, but with the accumulation of other triggers of cell death, possibly resulting from the type of DNA repair pathway chosen for DSB repair.

### DSBs repair pathway choice as a trigger of cell death in PARPi-treated BRCA1/2 deficient cells

The acquisition of resistance to PARPi has been mainly linked to the dysregulated activation of error-prone

repair pathways in BRCA-deficient cells (Lord and Ashworth, 2013). However, other mechanisms of resistance were also described. An indirect mechanism reported was the increased expression of genes that encode for the drug efflux transporter P-glycoprotein (Rottenberg *et al.*, 2008). Furthermore, the recovery of HR capacity (e.g., reversion of primary mutations or secondary mutations that restore BRCA function) promotes resistance to Olaparib (Edwards *et al.*, 2008; Sakai *et al.*, 2008; Swisher *et al.*, 2008; Norquist *et al.*, 2011). The loss of proteins that facilitate NHEJ activation, such as 53BP1, also promote resistance to PARPi and restoration of HR (Bunting *et al.*, 2010; Jaspers *et al.*, 2013). PTEN and Rev7 loss were additionally described as mechanisms of resistance driven by HR restoration (Peng *et al.*, 2014; Xu *et al.*, 2015). Besides the recovery of HR, stabilization of the replication fork by a limitation of exonuclease activity of MRE11 was reported as a trigger for PARPi resistance in BRCA-deficient backgrounds (Ray Chaudhuri *et al.*, 2016; Rondinelli *et al.*, 2017). Hence, PARPi resistance is linked to both the amount of DSBs formed and the loss of HR.

There is much less available evidence supporting that the dysregulation in DSBs repair also influences the extent of cell death caused by PARPi. The choice of alternative end joining (Alt-EJ) prevents cell death in PARPi-treated BRCA1-deficient cells (Ceccaldi *et al.*, 2015). Conversely, the elimination of pol  $\theta$  prevents ALT-EJ and increases cell death (Ceccaldi *et al.*, 2015). It is currently unknown whether such cell death is associated with the accumulation of persistent DSBs, or whether it depends on the HR-independent resolution of DSBs. Another factor to take into consideration when evaluating variables that influence the

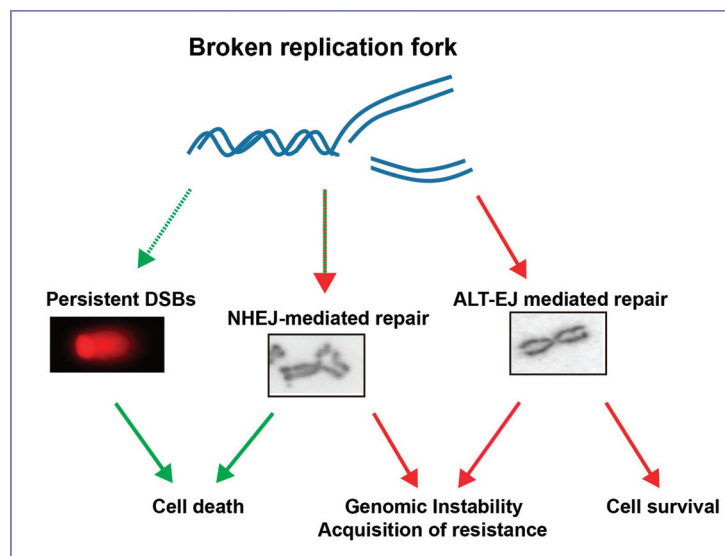


**Figure 5** - Model depicting the implications of low DSB accumulation after PARPi in BRCA-deficient cells. In BRCA-deficient cells, Olaparib treatment causes replication fork collapse. In rare samples, DSBs may accumulate and such a persistent load of DSBs may trigger cell death (left outcome). However, in most samples, DSBs are processed by error-prone pathways, such as non-homologous end joining (NHEJ) and alternative end joining (ALT-EJ). Error-prone pathways such as ALT-EJ, may not induce aberrant re-arrangement of chromosomes and may promote cell survival (middle outcome - see discussion). Other error-prone pathways that cause chromosome re-arrangement correlate with decreased cell survival (right outcome - see discussion).

survival of BRCA-deficient cells treated with PARPi is fork stabilization. ALT-EJ promotes fork stabilization and prevents its excessive processing (Kais *et al.*, 2016). Hence, the repair of DSBs via ALT-EJ promotes the survival of BRCA-deficient cells treated with PARPi. Intriguingly, the NHEJ-mediated repair of DSBs has the opposite effect on cell death induction. As a consequence of HR restoration, 53BP1 and Rev7 loss increases cell survival of PARP treated cells (Bunting *et al.*, 2010; Jaspers *et al.*, 2013; Xu *et al.*, 2015). It is therefore difficult to establish a causal link between chromosome instability and cell death. However, there are several correlations that put such a case into consideration. For example, FANCD2 loss increases both cell death and chromosome instability of BRCA2-deficient cells (Michl *et al.*, 2016). In addition, EZH2 depletion induces survival and prevents genomic instability in BRCA2-deficient tumors in a manner that depends on Mus81 loading to replication forks (Rondinelli *et al.*, 2017). PTIP loss also reduces both cell death and chromosome instability in BRCA1-deficient samples treated with PARPi, in this case without restoring HR (Ray Chaudhuri *et al.*, 2016). Moreover, expression of the micro RNA miR-493-5p affects the survival of PARPi-treated BRCA2-mutated/depleted cells by modulating the levels of nucleases involved in maintaining genomic stability and without affecting HR (Meghani *et al.*, 2018). Therefore, chromosome instability and cell death concomitantly occur in PARPi treated BRCA-deficient cells. As chromosome instability temporally precedes cell death it could be proposed that the trigger for cell death is a toxic upregulation of chromosomal instability. In fact, in the context of ATM deficiency, PARPi also induces cell death, which has been attributed to the accumulation of toxic NHEJ-generated aberrant chromosomes (Balmus *et al.*, 2019). Intriguingly, in such experimental settings, ATM-deficient cells do not accumulate DSBs, as revealed by a neutral comet assay (Balmus *et al.*, 2019). Hence, as in ATM-deficient cells, BRCA-deficient cells may die because of toxic chromosome instability triggered by PARPi.

#### Proofs of DSBs accumulation in BRCA-deficient cells treated with PARPi

Few assays can directly reveal DSBs, and such assays may not be very sensitive to low levels of DSBs. However, both pulse field gel electrophoresis (PFGE) and neutral comet assays can reveal DSBs reported to take place in HR-proficient settings (Elvers *et al.*, 2012; Murfuni *et al.*, 2013; Federico *et al.*, 2016; Quinet *et al.*, 2016). Such results suggest that the assays should be sensitive enough to detect DSBs in the context of HR-deficient cells. Intriguingly, such techniques were only rarely applied to BRCA-deficient cells treated with PARPi (Clements *et al.*, 2018; Gogola *et al.*, 2018). To our knowledge, this is the first report that uses a direct DSB detection method to explore the effect of the PARPi treatment on BRCA-depleted cells

(without the addition of other genotoxins). Instead of using direct DSBs detection, the PARPi field has chosen to focus its attention on the accumulation of  $\gamma$ H2AX nuclear foci as a marker of DSBs. Whether  $\gamma$ H2AX nuclear foci strictly correlate with DSBs accumulation is a subject of debate. Some laboratories have attempted to combine it with 53BP1 colocalization and to obtain independent evidence of DSBs formation, such as the accumulation of pATM and pKap1 (Berti *et al.*, 2013; Zellweger *et al.*, 2015; Federico *et al.*, 2016; Perkhofer *et al.*, 2017). However, the proof of DSBs formation is strictly dependent on the detection of such DNA lesions in PFGE or neutral comet assays. Multiple lines of evidence demonstrate that DSBs are formed after the PARPi treatment of BRCA-deficient samples. Most chromosome aberrations, as well as micronuclei, can only be formed from DSBs (Federico *et al.*, 2018). Moreover, the BRCAness signature is also associated with DSBs formation (Davies *et al.*, 2017). That being said, our data indicate that while DSBs are generated, they are not persistent enough to be the trigger for cell death as suggested by the currently accepted mode of action of PARPi. We hypothesize that DSBs are frequently formed but rapidly repaired by end-joining-mediated pathways after PARPi treatment. Perhaps in the future this hypothesis could be further evaluated by the modification of methods such as the NHEJ host reactivation assay, which needs to be adjusted according to the characteristics of PARPi-triggered DSBs (Nagel *et al.*, 2014). At least in this scenario,  $\gamma$ H2AX nuclear foci may rather reveal sites where DSB repair has occurred and sites of unresolved DSBs. These findings, therefore, suggest caution in the interpretation of  $\gamma$ H2AX foci data, a limitation that may extend to the analysis of other nuclear foci in the DNA damage response field.

#### Acknowledgments

This work was financially supported by Agencia Nacional de Promoción Científica y Tecnológica (ANPCyT) PICT2015-1217 and Instituto Nacional de Cancer to VG and PICT2016-0235 to GS. NP, MBdIV, IAG, and NLC were supported by fellowships from CONICET. MFP was supported by fellowships from the National Institute of Cancer and CONICET. GS and VG are researchers of CONICET. We would like to thank Anabel Alvarez Juliá and Andres H. Rossi for the excellent technical support in tissue culture and microscopy facilities.

#### Conflict of Interests

The authors declare no competing financial interests.

#### Author Contributions

GS and VG conceived and designed the study; NSP and VG designed the experiments; NSP, MBV, MFP, IAG and NLC generated tools and resources; NSP, MBV and

MFP performed the experiments; NSP, MBV, MP, IAG, NLC, GS and VG analyzed the data; VG wrote the original draft; NSP, MBV, GS and VG reviewed and edited the manuscript; all authors read and approved the final version.

## References

- Alexandrov LB, Nik-Zainal S, Siu HC, Leung SY and Stratton MR (2015) A mutational signature in gastric cancer suggests therapeutic strategies. *Nat Commun* 6:8683.
- Balmus G, Pilger D, Coates J, Demir M, Sczaniecka-Clift M, Barros AC, Woods M, Fu B, Yang F, Chen E *et al.* (2019) ATM orchestrates the DNA-damage response to counter toxic non-homologous end-joining at broken replication forks. *Nat Commun* 10:87.
- Berti M, Ray Chaudhuri A, Thangavel S, Gomathinayagam S, Kenig S, Vujanovic M, Odreman F, Glatter T, Graziano S, Mendoza-Maldonado R *et al.* (2013) Human RECQ1 promotes restart of replication forks reversed by DNA topoisomerase I inhibition. *Nat Struct Mol Biol* 20:347-354.
- Bryant HE, Schultz N, Thomas HD, Parker KM, Flower D, Lopez E, Kyle S, Meuth M, Curtin NJ and Helleday T (2005) Specific killing of BRCA2-deficient tumours with inhibitors of poly (ADP-ribose) polymerase. *Nature* 434:913-917.
- Bunting SF, Callen E, Wong N, Chen HT, Polato F, Gunn A, Bothmer A, Feldhahn N, Fernandez-Capetillo O, Cao L *et al.* (2010) 53BP1 inhibits homologous recombination in Brca1-deficient cells by blocking resection of DNA breaks. *Cell* 141:243-254.
- Bunz F, Dutriax A, Lengauer C, Waldman T, Zhou S, Brown JP, Sedivy JM, Kinzler KW and Vogelstein B (1998) Requirement for p53 and p21 to sustain G2 arrest after DNA damage. *Science* 282:1497-1501.
- Carbajosa S, Pansa MF, Paviolo NS, Castellaro AM, Andino DL, Nigra AD, Garcia IA, Racca AC, Rodriguez-Berdini L, Angiolini V *et al.* (2019) Polo-like Kinase 1 inhibition as a therapeutic approach to selectively target BRCA1-deficient cancer cells by synthetic lethality induction. *Clin Cancer Res* 25:4049-4062.
- Carlos AR, Escandell JM, Kotsantis P, Suwaki N, Bouwman P, Badie S, Folio C, Benitez J, Gomez-Lopez G, Pisano DG *et al.* (2013) ARF triggers senescence in Brca2-deficient cells by altering the spectrum of p53 transcriptional targets. *Nat Commun* 4:2697.
- Ceccaldi R, Liu JC, Amunugama R, Hajdu I, Primack B, Petalcorin MI, O'Connor KW, Konstantinopoulos PA, Elledge SJ, Boulton SJ *et al.* (2015) Homologous-recombination-deficient tumours are dependent on Poltheta-mediated repair. *Nature* 518:258-262.
- Clements KE, Thakar T, Nicolae CM, Liang X, Wang HG and Moldovan GL (2018) Loss of E2F7 confers resistance to poly-ADP-ribose polymerase (PARP) inhibitors in BRCA2-deficient cells. *Nucleic Acids Res* 46:8898-8907.
- Daley JM and Sung P (2014) 53BP1, BRCA1, and the choice between recombination and end joining at DNA double-strand breaks. *MOJ Cell Biol* 34:1380-1388.
- Davies H, Glodzik D, Morganella S, Yates LR, Staaf J, Zou X, Ramakrishna M, Martin S, Boyault S, Sieuwerts AM *et al.* (2017) HRDetect is a predictor of BRCA1 and BRCA2 deficiency based on mutational signatures. *Nat Med* 23:517-525.
- Edwards SL, Brough R, Lord CJ, Natrajan R, Vatcheva R, Levine DA, Boyd J, Reis-Filho JS and Ashworth A (2008) Resistance to therapy caused by intragenic deletion in BRCA2. *Nature* 451:1111-1115.
- Elvers I, Hagenkorf A, Johansson F, Djureinovic T, Lagerqvist A, Schultz N, Stoimenov I, Erixon K and Helleday T (2012) CHK1 activity is required for continuous replication fork elongation but not stabilization of post-replicative gaps after UV irradiation. *Nucleic Acids Res* 40:8440-8448.
- Fackenthal JD and Olopade OI (2007) Breast cancer risk associated with BRCA1 and BRCA2 in diverse populations. *Nat Rev Cancer* 7:937-948.
- Farmer H, McCabe N, Lord CJ, Tutt AN, Johnson DA, Richardson TB, Santarosa M, Dillon KJ, Hickson I, Knights C *et al.* (2005) Targeting the DNA repair defect in BRCA mutant cells as a therapeutic strategy. *Nature* 434:917-921.
- Federico MB, Vallerga MB, Radl A, Paviolo NS, Bocco JL, Di Giorgio M, Soria G and Gottifredi V (2016) Chromosomal integrity after UV irradiation requires FANCD2-mediated repair of double strand breaks. *PLoS Genetics* 12:e1005792.
- Federico MB, Campodonico P, Paviolo NS and Gottifredi V (2018) Beyond interstrand crosslinks repair: contribution of FANCD2 and other Fanconi Anemia proteins to the replication of DNA. *Mutat Res* 808:83-92.
- Feng W and Jasin M (2017) BRCA2 suppresses replication stress-induced mitotic and G1 abnormalities through homologous recombination. *Nat Commun* 8:525.
- Gogola E, Duarte AA, de Ruiter JR, Wiegant WW, Schmid JA, de Bruijn R, James DI, Guerrero Llobet S, Vis DJ, Annunziato S *et al.* (2018) Selective loss of PARG restores PARylation and counteracts PARP inhibitor-mediated synthetic lethality. *Cancer Cell* 33:1078-1093 e1012.
- Helleday T (2011) The underlying mechanism for the PARP and BRCA synthetic lethality: Clearing up the misunderstandings. *Mol Oncol* 5:387-393.
- Hock AK, Lee P, Maddocks OD, Mason SM, Blyth K and Vousden KH (2014) iRFP is a sensitive marker for cell number and tumor growth in high-throughput systems. *Cell Cycle* 13:220-226.
- Holter S, Borgida A, Dodd A, Grant R, Semotiuk K, Hedley D, Dhani N, Narod S, Akbari M, Moore M *et al.* (2015) Germline BRCA mutations in a large clinic-based cohort of patients with pancreatic adenocarcinoma. *J Clin Oncol* 33:3124-3129.
- Jaspers JE, Kersbergen A, Boon U, Sol W, van Deemter L, Zander SA, Drost R, Wientjens E, Ji J, Aly A *et al.* (2013) Loss of 53BP1 causes PARP inhibitor resistance in Brca1-mutated mouse mammary tumors. *Cancer Discov* 3:68-81.
- Johnson N, Johnson SF, Yao W, Li YC, Choi YE, Bernhardt AJ, Wang Y, Capelletti M, Sarosiek KA, Moreau LA *et al.* (2013) Stabilization of mutant BRCA1 protein confers PARP inhibitor and platinum resistance. *Proc Natl Acad Sci U S A* 110:17041-17046.
- Kais Z, Rondinelli B, Holmes A, O'Leary C, Kozono D, D'Andrea AD and Ceccaldi R (2016) FANCD2 maintains fork stability in BRCA1/2-deficient tumors and promotes alternative end-joining DNA repair. *Cell Rep* 15:2488-2499.
- Lord CJ and Ashworth A (2013) Mechanisms of resistance to therapies targeting BRCA-mutant cancers. *Nat Med* 19:1381-1388.

- Lord CJ and Ashworth A (2016) BRCAness revisited. *Nat Rev Cancer* 16:110-120.
- Lord CJ and Ashworth A (2017) PARP inhibitors: Synthetic lethality in the clinic. *Science* 355:1152-1158.
- Mansilla SF, Bertolin AP, Bergoglio V, Pillaire MJ, Gonzalez Besteiro MA, Luzzani C, Miriuka SG, Cazaux C, Hoffmann JS and Gottifredi V (2016) Cyclin Kinase-independent role of p21(CDKN1A) in the promotion of nascent DNA elongation in unstressed cells. *eLife* 5:e18020.
- Mauro M, Rego MA, Boisvert RA, Esashi F, Cavallo F, Jasin M and Howlett NG (2012) p21 promotes error-free replication-coupled DNA double-strand break repair. *Nucleic Acids Res* 40:8348-8360.
- Meghani K, Fuchs W, Detappe A, Drane P, Gogola E, Rottenberg S, Jonkers J, Matulonis U, Swisher EM, Konstantinopoulos PA *et al.* (2018) Multifaceted impact of microRNA 493-5p on genome-stabilizing pathways induces platinum and PARP inhibitor resistance in BRCA2-mutated carcinomas. *Cell Rep* 23:100-111.
- Michl J, Zimmer J, Buffa FM, McDermott U and Tarsounas M (2016) FANCD2 limits replication stress and genome instability in cells lacking BRCA2. *Nat Struct Mol Biol* 23:755-757.
- Murfuni I, Basile G, Subramanyam S, Malacaria E, Bignami M, Spies M, Franchitto A and Pichierri P (2013) Survival of the replication checkpoint deficient cells requires MUS81-RAD52 function. *PLoS Genetics* 9:e1003910.
- Nagel ZD, Margulies CM, Chaim IA, McRee SK, Mazzucato P, Ahmad A, Abo RP, Butty VL, Forget AL and Samson LD (2014) Multiplexed DNA repair assays for multiple lesions and multiple doses via transcription inhibition and transcriptional mutagenesis. *Proc Natl Acad Sci USA* 111:E1823-E1832.
- Norquist B, Wurz KA, Pennil CC, Garcia R, Gross J, Sakai W, Karlan BY, Taniguchi T and Swisher EM (2011) Secondary somatic mutations restoring BRCA1/2 predict chemotherapy resistance in hereditary ovarian carcinomas. *J Clin Oncol* 29:3008-3015.
- Peng G, Chun-Jen Lin C, Mo W, Dai H, Park YY, Kim SM, Peng Y, Mo Q, Siwko S, Hu R *et al.* (2014) Genome-wide transcriptome profiling of homologous recombination DNA repair. *Nat Commun* 5:3361.
- Perkhofer L, Schmitt A, Romero Carrasco MC, Ihle M, Hampp S, Ruess DA, Hessmann E, Russell R, Lechel A, Azoitei N *et al.* (2017) ATM deficiency generating genomic instability sensitizes pancreatic ductal adenocarcinoma cells to therapy-induced DNA damage. *Cancer Res* 77:5576-5590.
- Pommier Y, O'Connor MJ and de Bono J (2016) Laying a trap to kill cancer cells: PARP inhibitors and their mechanisms of action. *Sci Translat Med* 8:362ps317.
- Prakash R, Zhang Y, Feng W and Jasin M (2015) Homologous recombination and human health: the roles of BRCA1, BRCA2, and associated proteins. *Cold Spring Harb Perspect Biol* 7:a016600.
- Quinet A, Martins DJ, Vessoni AT, Biard D, Sarasin A, Stry A and Menck CF (2016) Translesion synthesis mechanisms depend on the nature of DNA damage in UV-irradiated human cells. *Nucleic Acids Res* 44:5717-5731.
- Ramus SJ and Gayther SA (2009) The contribution of BRCA1 and BRCA2 to ovarian cancer. *Mol Oncol* 3:138-150.
- Ray Chaudhuri A, Callen E, Ding X, Gogola E, Duarte AA, Lee JE, Wong N, Lafarga V, Calvo JA, Panzarino NJ *et al.* (2016) Replication fork stability confers chemoresistance in BRCA-deficient cells. *Nature* 535:382-387.
- Robinson D, Van Allen EM, Wu YM, Schultz N, Lonigro RJ, Mosquera JM, Montgomery B, Taplin ME, Pritchard CC, Attard G *et al.* (2015) Integrative clinical genomics of advanced prostate cancer. *Cell* 161:1215-1228.
- Rondinelli B, Gogola E, Yucel H, Duarte AA, van de Ven M, van der Sluijs R, Konstantinopoulos PA, Jonkers J, Ceccaldi R, Rottenberg S *et al.* (2017) EZH2 promotes degradation of stalled replication forks by recruiting MUS81 through histone H3 trimethylation. *Nat Cell Biol* 19:1371-1378.
- Rottenberg S, Jaspers JE, Kersbergen A, van der Burg E, Nygren AO, Zander SA, Derksen PW, de Bruin M, Zevenhoven J, Lau A *et al.* (2008) High sensitivity of BRCA1-deficient mammary tumors to the PARP inhibitor AZD2281 alone and in combination with platinum drugs. *Proc Natl Acad Sci USA* 105:17079-17084.
- Sakai W, Swisher EM, Karlan BY, Agarwal MK, Higgins J, Friedman C, Villegas E, Jacquemont C, Farrugia DJ, Couch FJ *et al.* (2008) Secondary mutations as a mechanism of cisplatin resistance in BRCA2-mutated cancers. *Nature* 451:1116-1120.
- Sun K, Mikule K, Wang Z, Poon G, Vaidyanathan A, Smith G, Zhang ZY, Hanke J, Ramaswamy S and Wang J (2018) A comparative pharmacokinetic study of PARP inhibitors demonstrates favorable properties for niraparib efficacy in pre-clinical tumor models. *Oncotarget* 9:37080-37096.
- Swisher EM, Sakai W, Karlan BY, Wurz K, Urban N and Taniguchi T (2008) Secondary BRCA1 mutations in BRCA1-mutated ovarian carcinomas with platinum resistance. *Cancer Res* 68:2581-2586.
- Talens F, Jalving M, Gietema JA and Van Vugt MA (2017) Therapeutic targeting and patient selection for cancers with homologous recombination defects. *Expert Opin Drug Discov* 12:565-581.
- Waddell N, Pajic M, Patch AM, Chang DK, Kassahn KS, Bailey P, Johns AL, Miller D, Nones K, Quek K *et al.* (2015) Whole genomes redefine the mutational landscape of pancreatic cancer. *Nature* 518:495-501.
- Xu G, Chapman JR, Brandsma I, Yuan J, Mistrik M, Bouwman P, Bartkova J, Gogola E, Warmerdam D, Barazas M *et al.* (2015) REV7 counteracts DNA double-strand break resection and affects PARP inhibition. *Nature* 521:541-544.
- Zellweger R, Dalcher D, Mutreja K, Berti M, Schmid JA, Herador R, Vindigni A and Lopes M (2015) Rad51-mediated replication fork reversal is a global response to genotoxic treatments in human cells. *J Cell Biol* 208:563-579.

*Associate Editor: Carlos F.M. Menck*

License information: This is an open-access article distributed under the terms of the Creative Commons Attribution License (type CC-BY), which permits unrestricted use, distribution and reproduction in any medium, provided the original article is properly cited.